Characterization and Three-Dimensional Structure Determination of ψ-Conotoxin PIIIF, a Novel Noncompetitive Antagonist of Nicotinic Acetylcholine Receptors[†,‡]

Ryan M. Van Wagoner,[#,§] Richard B. Jacobsen,[⊥] Baldomero M. Olivera,[⊥] and Chris M. Ireland*[,#]

Departments of Medicinal Chemistry and Biology, University of Utah, Salt Lake City, Utah 84112

Received December 2, 2002; Revised Manuscript Received March 25, 2003

ABSTRACT: A novel inhibitor of nicotinic acetylcholine receptors (nAChRs), ψ-conotoxin PIIIF, was isolated from the venom of *Conus purpurascens* and found to have the sequence GOOCCLYGSCROFOGCYN-ALCCRK-NH2. The sequence is highly homologous to that of ψ-conotoxin PIIIE, a previously identified noncompetitive inhibitor of *Torpedo* electroplax nAChR, also isolated from *C. purpurascens*. Both ψ-conotoxins block *Torpedo* and mouse nicotinic acetylcholine receptors (nAChRs), but ψ-PIIIF is less potent by a factor of 10^1-10^2. A high-resolution structure of ψ-PIIIF was determined by NMR and molecular modeling calculations. ψ-PIIIF analogues containing [^{13}C]-labeled cysteine at selected positions were synthesized to resolve spectral overlap of Cys side chain proton signals. The structures are well-converged, with backbone atom position RMSDs of 0.21 Å for the main body of the peptide between residues 4 and 22 and 0.47 Å for all residues. The overall backbone conformation is closely similar to ψ-PIIIE, the main difference being in the degree of conformational disorder at the two termini. ψ-PIIIE and ψ-PIIIF have similar locations of positive charge density, although ψ-PIIIF has a lower overall charge. One disulfide bridge of ψ-PIIIF appears to undergo dynamic conformational fluctuations based on both the model and on experimental observation. Chimeras in which the three intercysteine loops were swapped between ψ-PIIIE and ψ-PIIIF were tested for inhibitory activity against *Torpedo* nAChRs. The third loop, which contains no charged residues in either peptide, is the prime determinant of potency in these ψ-conotoxins.

Predatory gastropods of the genus *Conus* are among the most successful marine invertebrate animals. There are over 500 species of cone snail specialized, depending on the species, to feed on different types of prey, including fish, worms, or other snails (*1*, *2*). Every species of cone snail produces venom composed of neurotoxic peptides known as conotoxins that are as characteristic of the snails as their intricately patterned shells. The conotoxins are typically small (10−30 residues) and contain multiple disulfide bonds in each peptide that are believed to provide a well-defined conformation in solution. Each species of cone snail produces a complement of conotoxins (between 50 and 200 toxins per species) with a wide range of neurological targets. The fast action of the venom is critical for the survival of these predatory snails, which are often less mobile than their prey. Such rapidity is achieved by the use of an array of peptides with a myriad of molecular targets, by high potency and high selectivity in binding for each toxin, and by rapid diffusion of these typically small and hydrophilic peptides (*1*).

The first ψ-conotoxin, ψ-PIIIE,[1] recently isolated from the piscivorous cone snail *Conus purpurascens*, defined a new class of inhibitors of skeletal muscle nicotinic acetylcholine receptor (nAChR) with a mechanism of action that is apparently novel among venom-derived peptide inhibitors of the nAChR (*3*). Electrophysiological studies indicated an IC_{50} of 127 nM for ψ-PIIIE against *Torpedo* electroplax nAChR expressed on *Xenopus* oocytes. In terms of primary structure, the ψ-conotoxins most closely resemble the μ-conotoxins in the spacing of cysteine residues and the naturally occurring disulfide pairings (see Figure 1). The

† This work was supported by an NIH fellowship (GM08573) to R.M.V., by an American Foundation for Pharmaceutical Education predoctoral fellowship to R.M.V., and by an American Chemical Society Division of Medicinal Chemistry predoctoral fellowship funded by Pfizer to R.M.V.

‡ Atomic coordinates for the 17 converged structures of ψ-PIIIF have been deposited in the Protein Data Bank for release upon publication (accession code 1JLP).

* Corresponding author. Tel: (801) 581-8305. Fax: (801) 581-6208. E-mail: cireland@deans.pharm.utah.edu.

Department of Medicinal Chemistry.

⊥ Department of Biology.

§ Current address: Department of Biological Chemistry and Molecular Pharmacology, Harvard Medical School, 250 Longwood Ave., Boston, MA 02115, USA.

[1] Abbreviations: nAChR, nicotinic acetylcholine receptor; ψ-PIIIE, ψ-conotoxin PIIIE; O, *trans*-4-hydroxyproline; ψ-PIIIF, ψ-conotoxin PIIIF; Hyp, *trans*-4-hydroxyproline; HPLC, high-pressure liquid chromatography; C_{18}, octadecylsilyl reversed-phase chromatography; TFA, trifluoroacetic acid; CH_3CN, acetonitrile; A buffer, 0.1% TFA in water; B60, 60% CH_3CN, 0.092% TFA; B90, 90% CH_3CN, 0.08% TFA; LSIMS, liquid secondary ion mass spectrometry; fmoc, fluorenylmethoxycarbonyl; MTBE, methyl-*tert*-butyl ether; GSH, reduced form of glutathione; GSSG, oxidized form of glutathione; CH_3OH, methanol; MALDI-MS, matrix-assisted laser desorption ionization mass spectrometry; TRIS, tris-(hydroxymethyl)aminomethane; EDTA, ethylenediamine-*tetra*-acetic acid; ESIMS, electrospray ionization mass spectrometry; NOESY, nuclear Overhauser effect spectroscopy; HEPES, *N*-2-hydroxyethylpiperazine-*N*′-2-ethanesulfonic acid; ACh, acetylcholine; NMR, nuclear magnetic resonance; D_2O, deuterium oxide; TOCSY, total correlation spectroscopy, DQF−COSY, double quantum filtered correlation spectroscopy; PECOSY, primitive exclusive correlation spectroscopy; WET, water suppression enhanced through T_1 effects; NOESY−HSQC, three-dimensional nuclear Overhauser effect spectroscopy/heteronuclear single quantum coherence spectroscopy; FID, free induction decay; WATERGATE, water suppression by gradient tailored excitation; DGII, distance geometry II; IRMA, iterative relaxation matrix approach; CVFF, constant valence force field; RMSD, root-mean-squared deviation; i.m., intramuscular; nOe, nuclear Overhauser enhancement.

10.1021/bi0272757 CCC: $25.00
Published on Web 05/07/2003

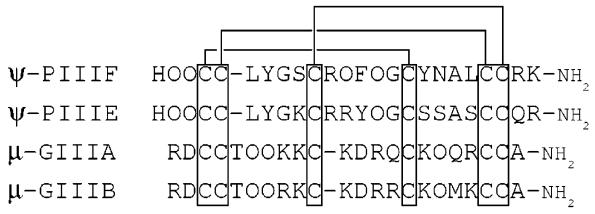

FIGURE 1: Sequence comparison of the μ-conotoxins and ψ-conotoxins. The μ-conotoxins block voltage-gated sodium channels and the ψ-conotoxins noncompetitively inhibit nAChR. O = *trans*-4-hydroxyproline; -NH_2 = amidated C-terminus.

μ-conotoxins, however, target the voltage-gated Na^+ channel and have no inhibitory activity against the nAChR.

We describe the isolation and structural characterization of a newly discovered ψ-conotoxin designated ψ-PIIIF. ψ-PIIIF is only partially homologous to and significantly less potent than ψ-PIIIE, providing an opportunity for insight into the structural basis for the activity of these peptides. As part of a program comparing the structures and activities of these two ψ-conotoxins, we undertook a structural determination of ψ-PIIIF and tested the activity of a series of synthetic chimeric peptides in which portions of sequence from the two ψ-conotoxins were combined. Although ψ-PIIIE and ψ-PIIIF are highly homologous in sequence (15/24 residues are identical), there are significant differences such as replacement of Arg with Hyp at position 12 in ψ-PIIIF (see Figure 1) that might have strong effects on backbone conformation and not merely on surface topology. We were able to use methods developed earlier with ψ-PIIIE (*4*) of incorporating ^{13}C-labeled cysteine at selected positions as a means of resolving resonance overlap problems for cysteine residues and allowing more precise specification of cysteine side chain conformation. While the resulting structures are similar in overall conformation to ψ-PIIIE, the structural models of ψ-PIIIF indicate differences in dynamic motion in comparison to ψ-PIIIE that would not necessarily be detected by sequence comparison alone.

EXPERIMENTAL PROCEDURES

Reversed-Phase High-Pressure Liquid Chromatography (HPLC). Most of the analytical HPLC of synthetic peptides was performed using a Hewlett-Packard 1090 chromatograph with diode array detection. A Rainin analytical C_{18} HPLC column (4.6 mm × 25 cm; 100 Å pore size; 1 mL/min flow rate) was used for screening of reaction conditions and preparative column fractions. Large scale purification of the peptides was achieved using Rainin preparative C_{18} HPLC columns (21.4 mm × 25 cm, 60 Å pore size; 10 mL/min flow rate). The purification of native ψ-PIIIF and the FEE- and EFE-PIIIE chimeras was performed using Vydac analytical (4.6 mm × 25 cm, 5 μ particle size, 300 Å pore size) and preparative (22 mm × 25 cm, 15 μ particle size, 300 Å pore size) C_{18} columns. Sequencing grade trifluoroacetic acid (TFA) was obtained from Aldrich and UV grade acetonitrile (CH_3CN) was obtained from Fisher. HPLC buffers consisted of 0.1% TFA in H_2O (A buffer), 0.092% TFA and 60% CH_3CN in H_2O (B60 buffer) and 0.08% TFA and 90% CH_3CN in H_2O (B90 buffer).

Isolation of ψ-PIIIF from C. purpurascens Venom. Specimens of the purple cone, *C. purpurascens*, were collected from Clipperton Island in the eastern Pacific. The venom

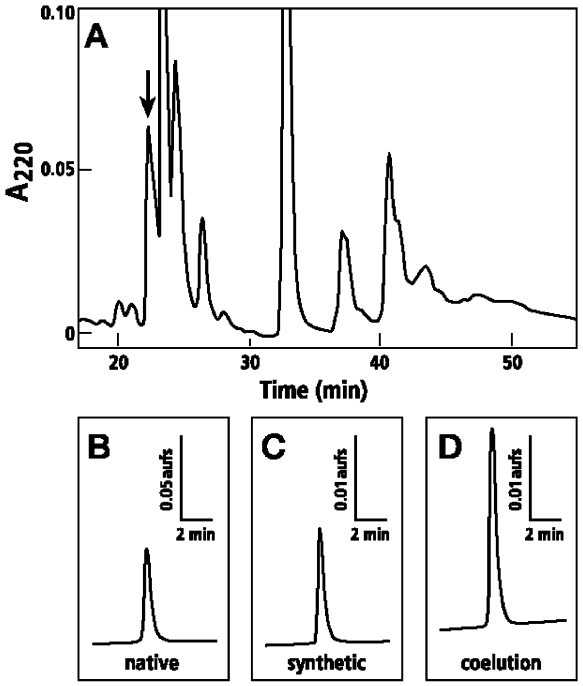

FIGURE 2: Purification and coelution of ψ-PIIIF. (A) ψ-PIIIF was purified from the milked venom of *C. purpurascens* specimens from the Clipperton Islands. A portion of the reverse phase preparative HPLC chromatogram produced during a 0−100% gradient of B90 buffer over 100 min is shown. (B) The peak indicated by an arrow in (A) was further purified by analytical HPLC. (C) Synthetic ψ-PIIIF eluted under identical HPLC conditions. (D) Coelution of equal amounts of synthetic and native peptide. All analytical HPLC used a 20−50% gradient of B60 buffer over 30 min. In B−D, only the portion of the gradient from 12 to 20 min is shown.

was acquired by milking snails kept in aquaria, as previously described (*5*). The snails were milked 1−2 times per week (yielding 5−10 μL/milking) and milked venom was stored at −70 °C. The venom from ∼70 milkings (∼0.5 mL) was pooled for large-scale purification. The venom was diluted (∼200-fold) with A buffer and purified by preparative HPLC using a 0−100% gradient of B90 buffer over 100 min. A crude fraction from preparative purification was further purified on an analytical HPLC column using a shortened gradient of B60 buffer (see Figure 2).

Sequence Analysis and Mass Spectrometry. Purified, native peptide was reduced with tris-(2-carboxyethylphosphine), HPLC-purified, and then alkylated with 4-vinyl pyridine as described by Gray to determine the disulfide bonding pattern (*6*). The pyridylethylated peptide was purified by HPLC and analyzed by automated Edman degradation on an ABI model 477A sequencer. The peptide sequence and C-terminal amidation were confirmed by positive ion LSIMS using a JEOL JMS HX110 double-focusing spectrometer fitted with a cesium ion gun operated at +30 kV.

Peptide Synthesis. Linear peptides were built on Rink amide resin using standard fmoc chemistry. Amino acid side chains were protected as previously described (*5*). The cysteine residues were differentially protected as a part of the folding strategy. Cysteine residues 4, 5, 16, and 21 were protected as acid-labile trityl thioethers. Cysteine residues 10 and 22 were protected as acetamidomethyl sulfides. At the completion of synthesis, the terminal fmoc group was removed in situ by treatment with 20% piperidine in *N*-methylpyrrolidone.

Linear ψ-PIIIF was cleaved from resin by treatment with TFA/H_2O/ethanedithiol/phenol/thioanisole (90/5/2.5/7.5/5 by volume) for 3−4 h at 22 °C. The peptide cleavage product and a 1 mL TFA rinse of the reaction tube were filtered into 200 mL of stirring methyl-*tert*-butyl ether (MTBE) cooled to −10 °C. The precipitate was collected by low-speed centrifugation and washed twice with cold MTBE. The supernatant was discarded and the pellet was dissolved in 10−20 mL of B60 buffer. Linear peptide was then purified by preparative C_{18} HPLC using a gradient of 25−55% B60 (60% CH_3CN, 0.092% TFA) in A buffer over 30 min (2.2 × 25 cm; flow rate 20 mL/min). Oxidation by incubation of the peptide in a 0.1 M pH 7.7 phosphate buffer solution containing 1.0 mM GSH and 0.5 mM GSSG for 12−16 h at room temperature was followed by quenching with TFA and preparative C_{18} HPLC purification (20−50% B60 in A buffer over 30 min). The isolate from the preparative column (35 mL volume) was added dropwise to 50 mL of a stirring solution of 5 mM I_2 (10% CH_3OH, 20% CH_3CN, 2% TFA, 68% water). The mixture was stirred for 10 min followed by quenching of the remaining I_2 with ascorbic acid to cause deprotection and oxidation of the remaining cysteine residues. The fully folded toxin was purified using a 20−50% B60 gradient over 30 min. The isolate from the column was found to comigrate by analytical HPLC with authentic ψ-PIIIF using a 20−50% B60 gradient over 30 min. The synthetic peptide was also tested for toxicity in goldfish. MALDI-MS gave an average molecular mass ($[MH]^+$) of 2667.68 Da (calculated 2667.21 Da). The total yield from 500 mg of resin was 31.7 mg of peptide (10.1 μmol of the tetra-TFA salt of ψ-PIIIF).

Synthesis, Folding, and Purification of ψ-PIIIE/ψ-PIIIF Chimeras. Chimeras were synthesized as linear peptides and removed from resin as described above. It was found previously that ψ-PIIIE could be oxidized in a single step using glutathione (*3*). Those chimeras that contained two loops from ψ-PIIIE were produced in this way. Chimeras containing two loops from ψ-PIIIF were synthesized using the same protecting group and two-step oxidation strategies used for ψ-PIIIF. All GSSG/GSH or cystamine/GSH folding mixtures contained 100 mM TRIS (pH 8.0) and 10 mM EDTA. Folding reactions were quenched by the addition of 1/10th volume of formic acid prior to purification. The linear and oxidized peptides were typically eluted during gradients between 20 and 60% B60 buffer using preparative HPLC as described above (10−20 mL/min flow rate, 0.5% B60 buffer increase/min). The masses of synthetic peptides were confirmed by ESIMS. The oxidation conditions for each chimeric peptide were optimized and varied slightly as summarized: FEE-PIIIE, 1 mM cystamine/1 mM GSH, 1 h at 4 °C; EFE-PIIIE, 1 mM GSSG/1 mM GSH, 1 h at 22 °C; EEF−PIIIE, 1 mM cystamine/1 mM GSH, 100 min at 22 °C; EFF−PIIIF, 1 mM GSSG/2 mM GSH, 23 h at 22 °C; FEF−PIIIF, 1 mM cystamine/1 mM GSH, 23 h at 4 °C; FFE-PIIIF, 2 mM cystamine/1 mM GSH, 2 h at 4 °C. The yields of folded peptide from 200 mg of resin were FEE-PIIIE, 3.5 mg; EFE-PIIIE, 2.7 mg; EEF−PIIIE, 8 mg; EFF−PIIIF, 3.8 mg; FEF−PIIIF, 4.4 mg; FFE-PIIIF, 2.8 mg.

Synthesis of C4-(3-[^{13}C]-Cysteine)-ψ-PIIIF. 99% [3-^{13}C]-*N*-(9-fluorenylmethoxycarbonyl)-*S*-trityl-L-cysteine was synthesized as previously described (*7*, *8*) using 99% [3-^{13}C]-L-cysteine (Cambridge Isotope Laboratories, CLM-1868). The labeled amino acid was incorporated into position C4 of ψ-PIIIF using fmoc-based solid-phase chemical synthesis (50 μmol scale). The ^{13}C-labeled residue was reacted with the resin at a 5-fold excess and the natural isotopic abundance residues were reacted at a 10-fold excess. Partial deprotection and purification of the linear peptide were accomplished by procedures similar to natural abundance ψ-PIIIF except that a gradient of 30−60% B60 over 30 min was utilized. Oxidation in a buffered solution (0.1 M TRIS, 1 mM EDTA, 1 mM GSH, 1 mM cystamine dihydrochloride, pH 8.0) at 4 °C for 2 h was followed by quenching with formic acid and purification by preparative C_{18} HPLC with a 25−55% gradient of B60 in 0.1% TFA over 60 min (10 mL/min). Deprotection and oxidation by iodine as described above were followed by preparative C_{18} HPLC (20−50% gradient of B60 over 60 min; 10 mL/min) to yield the correctly folded peptide as confirmed by comparison with authentic ψ-PIIIF of NOESY spectra. The yield was 24.2 mg from 250 mg of resin (7.75 μmol of the tetra TFA salt). ESIMS indicated a chemical mass of 2668.0 Da for $[MH]^+$ (calculated 2668.1 Da).

Bioassay. Biological activity was measured by injection into the anterior region of the ventral fin of goldfish (0.7−0.9 g). Aliquots of ψ-conotoxin in 5 μL of normal saline solution were injected using a 0.3 mL syringe with a 29-gauge needle. Each control fish was injected with normal saline solution containing dissolved residue of lyophilized column buffer. After injection, the fish were placed in aquaria for observation.

Expression and Electrophysiology in Xenopus Oocytes. The preparation of mRNA and injection into oocytes of *Xenopus laevis* were previously described (*3*). Oocytes were used for electrophysiological measurements 16−60 h after injection. The oocytes were immobilized in a well with a volume of 30 μL continually perfused with a solution of ND96A (96.0 mM NaCl, 2.0 mM KCl, 1.8 mM $CaCl_2$, 1.0 mM $MgCl_2$, 5 mM HEPES, pH 7.1−7.5, 1 μM atropine; gravity perfusion, 2 mL/min). The membrane of the oocyte was pierced with two glass electrodes filled with 3 M KCl connected to a voltage-clamp amplifier set to fast clamp mode. Application of acetylcholine (ACh) to the oocyte was achieved through a system of voltage-controlled solenoids in the solvent flow path. The response of the oocyte to a 1 s application of a solution of ND96A containing 1 μM ACh was measured in constant voltage mode. For each measurement, a 1 s pulse of ACh was applied at 1-min intervals until a steady response was achieved. The flow of the bath was then stopped and 5 μL of a solution of the peptide being tested in ND96A was added to the well. The oocyte was maintained in this well for 5 min prior to resumption of flow and immediate application of ACh to determine the effect of the incubation on the transmembrane current that develops in response to ACh. The flow and application of ACh every min were continued until a steady response to ACh was again achieved. The percentage of response after incubation with toxin was taken as the ratio of the response immediately after incubation to an average of the three measurements prior to the application of toxin. Control measurements were performed by incubation of the oocyte in a static bath containing no toxin. Three replicate measurements were taken for each peptide at each concentration tested. All replicate measurements for the ~10 μM concentration set of all peptides tested were taken on a single oocyte. Similarly, a single oocyte

was used for all measurements of the ~200 nM concentration set of all peptides.

NMR Data Acquisition. All data were acquired using a 5-mm NMR microtube with insert matched to D_2O (Shigemi Co., Ltd.) on a Varian UNITY 500 MHz spectrometer with a 5-mm gradient-capable Nalorac triple resonance probe or on a Varian INOVA 600 MHz spectrometer with a gradient-capable Nalorac triple resonance probe. For NMR studies 9.1 mg of natural isotopic abundance ψ-PIIIF (2.9 μmol assuming the tetra-TFA salt form) were dissolved in 250 μL of a 9:1 water/D_2O solution to give a nominal peptide concentration of 12 mM. The pH of the solution was adjusted to an uncorrected value of 3.5 using TFA. The pulse sequences used for NOESY (*9*), TOCSY (*10*), DQF−COSY (*11*), and PECOSY(*12*) were similar to those previously described. WET (*13*) suppression was applied prior to frequency labeling for DQF−COSY and TOCSY experiments, and at the end of the mixing period in NOESY. Quadrature discrimination of frequencies in the indirectly detected dimension was achieved in all experiments through use of States hypercomplex acquisition (*14*). For isotopically labeled ψ-PIIIF, 24.2 mg of peptide were dissolved in 500 μL of a solution containing 9:1 water/D_2O, pH 3.5 (TFA) to give an approximate concentration of 16 mM peptide. NMR experiments include a ^{13}C-selected NOESY, a doubly ^{13}C-filtered (*15*) NOESY, a TOCSY, and a DQF−COSY. The ^{13}C-selected NOESY spectrum was acquired as a two-dimensional version of a NOESY−HSQC (*16*) using a mixing time of 150 ms. Experiments were typically acquired at 4 and 22 °C. A table in the Supporting Information provides the details of acquisition parameters.

For each chimeric peptide NOESY, TOCSY, and DQF−COSY experiments utilizing either WET or WATERGATE (*17*) methods of solvent suppression were used. The parameters for these experiments were similar to those used for ψ-PIIIF. The concentrations of peptide varied between 8 and 25 mM. Chemical shift referencing was achieved by assigning the center of the water resonance to be δ 4.93 ppm to allow direct comparison to the chemical shift values of ψ-PIIIE and ψ-PIIIF. For experiments collected at temperatures other than 4 °C, the reference shift for water was calculated from the expected temperature dependence of the chemical shift of water (*18*).

Data Processing. All NMR data sets were analyzed using either VNMR (Varian, Inc.) or FELIX (Accelrys, Inc). TOCSY, DQF−COSY, and NOESY experiments were zero-filled once in D1 and three times in D2 to give final matrixes consisting of 4096 by 2048 real points with resolution values of 1.4 and 2.8 Hz/pt for the D1 and D2 vectors, respectively. For NOESY and TOCSY spectra, t_2 FIDs and t_1 interferograms were processed by convolution with 90° phase-shifted sinebell squared curves (with widths of 2048 and 1024 points, respectively) prior to complex fast Fourier transformation. DQF−COSY spectra were processed with 60° phase-shifted sinebell squared curves in t_2 (2048 point width) and t_1 (1024 point width) prior to transformation. The PECOSY data set was processed by zero-filling once in D1 and three times in D2 to give a final matrix of 8192 by 2048 real points and resolution values of 0.7 and 2.8 Hz/pt for the D1 and D2 vectors. Apodization and resolution enhancement were achieved by convolution with 60° phase-shifted sinebell window functions with widths of 4096 points (in t_2) and 512 points (in t_1) prior to transformation. Baseline correction was applied in both dimensions of NOESY and TOCSY experiments to enhance detection of cross correlations and increase the accuracy of volume measurement. Automatic baseline detection was achieved by use of the FLATT algorithm (*19*) with default parameters as provided by FELIX.

Determination of Restraints and Molecular Modeling. All calculations were performed using the Insight II 97.0 suite of programs (Accelrys, Inc). Molecular dynamics calculations were performed using DISCOVER 2.98 (Accelrys, Inc.) and DGII 97.0 (Accelrys, Inc.) was used for distance geometry calculations. Distance restraints for the highest quality NOESY cross-peaks were calculated using standard IRMA (Accelrys, Inc.) methodology (*20*, *21*). Lower quality cross-peaks were classified according to cross-peak intensity into the following restraints: strong (1.5−2.5 Å), medium (2.5−3.5 Å), weak (3.5−5.0 Å), and very weak (3.5−6.0 Å). The dihedral angle ϕ was restrained to values of −90° to −40° for $^3J_{HNH\alpha} < 5$ Hz and to the range −160° to −80° for $^3J_{HNH\alpha} > 8$ Hz (*22*). Restraints on χ^1 were restricted to be ±15° of the values determined according to the method of Hyberts et al (*23*). The disulfide bonding pattern, as determined experimentally, was enforced through explicit covalent bonds prior to metric matrix embedding. The final structures were generated by distance geometry calculations followed by simulated annealing and energy minimization using standard protocols (*24*, *25*). Potential energy terms were derived from the CVFF (*26*). The force constants were set to values of 20.00 kcal (mol Å^2)$^{-1}$ for all distance restraints and 30.00 kcal (mol radian^2)$^{-1}$ for dihedral angle restraints. Electrostatic potentials were disregarded for all modeling calculations due to the use of in vacuo conditions. Figures were generated using the program MOLMOL 2k.2 (*27*) in conjunction with the program POV−Ray for rendering.

RESULTS

Characterization of a ψ-Conotoxin from Clipperton Island Specimens of C. purpurascens. Pooled milked venom from *C. purpurascens* was analyzed using a reversed-phase HPLC system previously shown to be effective for separating peptides from *C. purpurascens* venom (*3*). The first major peak that eluted from the column (see Figure 2A,B) was purified to homogeneity.

The peak was reduced, alkylated, and characterized by Edman sequencing and MALDI-MS as detailed in Experimental Procedures. The sequence analysis identified all 24 residues and the pattern of disulfide bonding for all three cystine bridges. MALDI-MS gave a monoisotopic $[MH]^+$ mass of 2667.68 Da. The results are consistent with the sequence assignment for the peptide given in Figure 1 (the amidated peptide has a predicted monoisotopic MH^+ mass = 2667.21 Da). On the basis of the strong sequence homology between this peptide and the previously characterized ψ-PIIIE from *C. purpurascens* specimens collected in the Gulf of California (see Figure 1), we have named the new peptide ψ-conotoxin PIIIF. Nevertheless, the degree of sequence divergence between these peptides (9 of 18 noncysteine residues are different) is unprecedented for *Conus* peptides isolated from what are believed to be variants of the same species.

Chemical Synthesis of ψ-PIIIF and Comparison of Biological Activity to ψ-PIIIE. To further characterize ψ-PIIIF, the

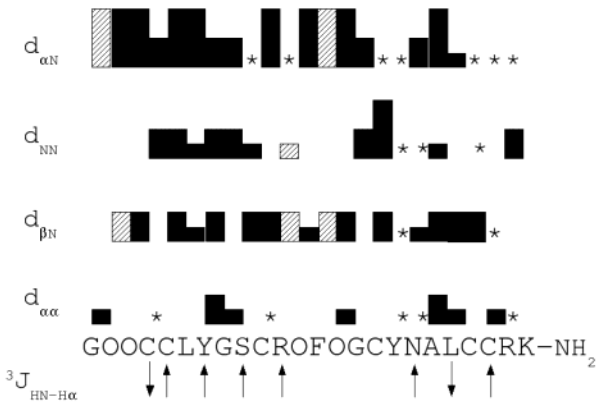

FIGURE 3: Sequential connectivities for ψ-PIIIF. The height of each block is proportional to the strength of the nOe interaction. A "*" denotes problems with resonance overlap. Boxes with hash marks indicate correlations with δ protons of Hyp rather than with amide protons. ↑ = $^3J_{HNH\alpha}$ > 8 Hz and ↓ = $^3J_{HNH\alpha}$ < 5 Hz.

peptide was chemically synthesized. The synthetic peptide comigrated with native peptide when equal amounts were mixed and eluted by reversed-phase HPLC (see Figure 2B–D). The biological activity of synthetic and native ψ-PIIIF was also found to be identical, causing flaccid paralysis and death following i.m. injection into goldfish at dosages above 50 pmol (or 42 pmol/g of body weight). The potencies of synthetic ψ-PIIIF and ψ-PIIIE were directly compared using the goldfish assay and found to be nearly identical. Subsequent electrophysiological studies were performed with synthetic ψ-conotoxins.

The potency of the ψ-conotoxins were also compared using oocyte-expressed nAChRs. Two concentrations were tested for each peptide by static bath application to oocytes expressing either the mouse muscle (γ-containing; 20 and 200 μM toxin) or *Torpedo* subtype (0.2 and 10 μM toxin) of nAChR. The apparent IC_{50} values for ψ-PIIIE in this assay (20 μM mouse, 177 nM Torpedo) are consistent with previously published values (14 μM mouse, 127 nM *Torpedo*) (*3*) and are roughly 50 to 100-fold more potent than ψ-PIIIF (~1 mM mouse, 19 μM *Torpedo*). As a first step toward identifying the structural basis for the difference in potency between ψ-PIIIE and ψ-PIIIF, we constructed chimeric peptides with portions of sequence from each toxin as described later in this article.

Determination of the Three-Dimensional Structure of ψ-PIIIF by NMR– Assignment of ^{1}H Resonances, Determination of Restraints on Dihedral Angle, and Stereospecific Assignment. Assignments were made for all observed ^{1}H resonances according to the methodology of Wüthrich (*28*). The method of Hyberts et al. (*23*) was used to determine restraints on χ^1 based on the observed intraresidue nOe and scalar coupling interactions. Restraints on χ^1 were determined for C4, C5, Y7, R11, F13, C16, and C21. This analysis allowed the determination of stereospecific restraints for the prochiral side chain hydrogen atoms of residues C4, C5, Y7, R11, F13, C16, N18, and C21. Analysis of the pattern of intraresidue nOe interactions for hydroxyproline residues (*24*) led to stereospecific assignment of prochiral β hydrogen atoms of residues O2, O3, O12, and O14, and the δ hydrogen atoms of O14. Restraints on ϕ were determined from measurement of $^3J_{HNH\alpha}$ (Figure 3).

Design of a Selectively ^{13}C-Labeled Derivative of ψ-PIIIF. A preliminary structural ensemble produced by molecular

Table 1: Restraints Used for the Structure Determination of ψ-PIIIF

distance restraints	
intraresidue	121
sequential	121
medium	55
long	31
total	328
dihedral restraints	
ϕ	7
χ^1	7
total	14

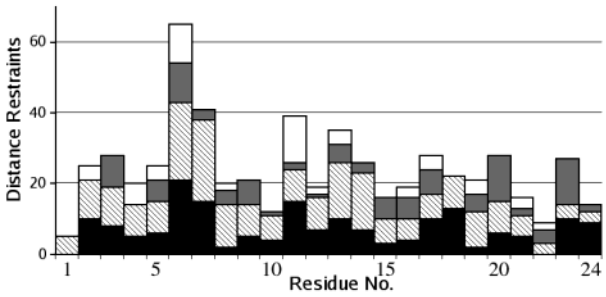

FIGURE 4: Distribution of distance restraints across the sequence of ψ-PIIIF. Black bars indicate intraresidue restraints, crosshatched bars indicate sequential restraints, gray bars indicate restraints between residues separated by 2–4 amino acids, and white bars indicate long-range distance restraints.

modeling calculations utilizing a fully refined restraint set for ψ-PIIIF produced two families of structures in these studies. The two structural families differed from each other on the basis of the χ^1 angle for C4, one of the cysteine residues for which χ^1 restraints could not be specified due to problems of resonance overlap. The NMR data indicated that C4 was rotationally static and in a staggered conformation, but the data did not provide unambiguous support for one structural family over the other, even after iterative refinement of the distance restraints. On the basis of the successful use of selective ^{13}C-labeling of cysteine residues to resolve resonance overlap problems in the structure determination of ψ-PIIIE (*4*), ψ-PIIIF that incorporated 3-^{13}C-labeled Cys at position 4 was synthesized as a means of resolving the overlap problems for C4, C5, and C10. The use of ^{13}C-selected and ^{13}C-filtered NMR experiments previously employed for the structure revision of ψ-PIIIE allowed the determination of restraints on χ^1 for C4 and C5. For C10, however, the measured parameters were not consistent with a static, staggered conformation of χ^1.

Structure Calculations and Evaluation for ψ-PIIIF. Data for both the ^{13}C-labeled and natural isotopic abundance peptides allowed the identification of 328 nonredundant distance restraints (as determined by the program AQUA (*29*)), seven restraints on ϕ, and seven restraints on χ^1 for ψ-PIIIF (see Table 1 and Figure 4) that were used as input for a molecular modeling protocol similar to that used for ψ-PIIIE (*24*) to generate 50 structures, 17 of which were found to converge by analysis of residual restraint violations and by energy calculations. The structures of ψ-PIIIF show fairly low amounts of circular variance for ϕ and ψ of residues 1–22. The RMSD values, R_1 factor, and deviation of bond lengths and bond angles from ideal values all indicate that the structures are well-converged and consistent with normal protein geometry (see Table 2). The RMSD from dihedral angle restraints is also low indicating consistency with the

Table 2: Energetic and Structural Statistics for ψ-PIIIF

RMSD for C^{α}, N, C atoms from average molecule coordinates (Å)	
residues 4−22	0.21
all residues	0.47
RMSD from distance restraints (Å)	0.119
RMSD from dihedral restraints (deg)	1.32
R_1 for ensemble	0.396
RMSD from idealized geometry	
bond lengths (Å)	0.0147 ± 0.001
bond angles (deg)	2.21 ± 0.03
energies (kcal mol^{-1})	
$E_{restraint}$	108 ± 7
E_{L-J}	181 ± 3
$E_{bond} + E_{angle} + E_{improper}$	245 ± 5
Ramachandran plot statistics (%)	
residues in most favored region	76
residues in additionally allowed region	23
residues in generously allowed region	0.7
residues in nonallowed region	0

FIGURE 5: Defocused stereoviews of the 17 converged structures of ψ-PIIIF produced by simulated annealing calculations. All structures are aligned with the N-terminus toward the top of the figure and the C-terminus toward the bottom. Only the heavy atoms are shown for all residues. The side chains of basic residues are blue.

Table 3: Secondary Structure Elements Present in ψ-PIIIF

residues	structural element
O3−L6	Type VIII β turn
L6−S9	Type I′ β turn
O12−G15	Type VIII β turn
F13−C16	Type II β turn
C16−A19	Type III β turn
A19−C22	Type III β turn

data. A majority of the residues (76%) have $\phi-\psi$ combinations that occur in the most favored regions of the Ramachandran plot as identified by PROCHECK_NMR (*29*).

Three-Dimensional Structure. The converged structures of ψ-PIIIF are shown in Figure 5. Residues having less than 20% solvent surface area exposure (as determined by MOLMOL 2k.2) include C4, C5, L6, F13, C16, A19, and C22. These residues can be considered to constitute the hydrophobic core of ψ-PIIIF. The side chain of A19 in particular packs close to the disulfide core. The hydrophobic residue L20, on the other hand, is ~50% exposed to solvent. Residues having >60% solvent exposure include G1, Y7, and K24. There are no β sheet regions longer than two residues in the models. The backbone does adopt a roughly helical conformation near the C-terminus and the secondary structure detection algorithm of MOLMOL 2k.2 indicates the presence of a single turn of a 3_{10} helix between residues 20 and 22 in 7 of the 17 structures. The remaining secondary structure of ψ-PIIIF can best be described as a series of reverse turns. The types of reverse turns observed are listed in Table 3. The amide hydrogens implicated as participants in hydrogen bonding by the models (see Supporting Information) exhibited slow exchange in D_2O, as did a number of amide hydrogens not involved in hydrogen bonds in the models.

Table 4: Sequence and Potency of ψ-PIIIE/ψ-PIIIF Chimeras against *Torpedo* nAChR with Standard Deviation

	IC_{50} (μM), (SD)	sequence
ψ-PIIIE	0.177 (0.003)	HOOCCLYGKCRRYOGCSSASCCQR−NH_2
FEE−PIIIE	0.05 (0.01)	HOOCCLYGSCRRYOGCSSASCCQR−NH_2
EFE−PIIIE	0.37 (0.02)	HOOCCLYGKCROFOGCSSASCCQR−NH_2
EEF−PIIIE	0.98 (0.06)	HOOCCLYGKCRRYOGCYNALCCQR−NH_2
ψ-PIIIF	19 (0.9)	GOOCCLYGSCROFOGCYNALCCRK−NH_2
EFF−PIIIF	6.7 (0.5)	GOOCCLYGKCROFOGCYNALCCRK−NH_2
FEF−PIIIF	16.3 (0.5)	GOOCCLYGSCRRYOGCYNALCCRK−NH_2
FFE−PIIIF	0.033 (0.002)	GOOCCLYGSCROFOGCSSASCCRK−NH_2

Chimeric Peptides: Synthesis and Structural Analysis. Systematic exchange of the internal loop regions between ψ-PIIIE and ψ-PIIIF produces six chimeric peptides, the nomenclature and sequences of which are given in Table 4. These peptides were chemically synthesized and folded as described in the Experimental Procedures.

Comparison of chemical shift values of the chimeras to those of ψ-PIIIE and ψ-PIIIF was used to confirm formation of the correct native disulfide bridge bonding pattern and provide a measure of the structural similarities between chimeric and parent peptides. While the complete NMR structure determination of the six chimeric peptides would be a substantial undertaking, the availability of high-resolution structures and complete assignments for the two parent peptides (ψ-PIIIE and ψ-PIIIF) allows at least a rough estimation of the structures of the chimeric conotoxins. A previous study exploring the determinants of calcium channel subtype selectivity within the ω-conotoxins similarly produced a series of loop-swapped hybrid peptides and made use of ^{1}H NMR chemical shift as a means of confirming formation of the native disulfide bridge folding pattern (*30*).

The ^{1}H NMR chemical shift of a given proton resonance is sensitive to the local structural environment. Thus, a comparison of chemical shift can provide information about the similarity in conformation between related molecules (*31*). Determination of resonance assignments for the chimeric peptides required the collection of data from various TOCSY, DQF−COSY, and NOESY experiments. Resonance-specific assignments were made according to the procedures of Wüthrich (*28*). The general procedure used was to construct spin systems from the TOCSY data, to identify the likely location of these spin systems in the peptide by comparison to the chemical shift assignments for ψ-PIIIE and ψ-PIIIF, and to confirm the assignments with the sequential interresidue cross-peaks observed in the NOESY spectra. Further confirmation was achieved by examination of the DQF−COSY spectra for consistency with the proposed assignments. The data were then compared to both ψ-PIIIE and ψ-PIIIF through the calculation of the RMSD for variation in chemical shift of the chimeras against either parent peptide for each residue. The data were further analyzed for the occurrence of chemical shift degeneracy for diastereotopic protons such as the side chain β protons of cysteine residues to provide information on the rotational dynamics of these residues. Additionally, other indicators of dynamics such as unusually broad line widths were also evaluated in the NMR data.

Chemical shift RMSD plots of the various chimeric peptides in comparison to ψ-PIIIE and ψ-PIIIF are shown in

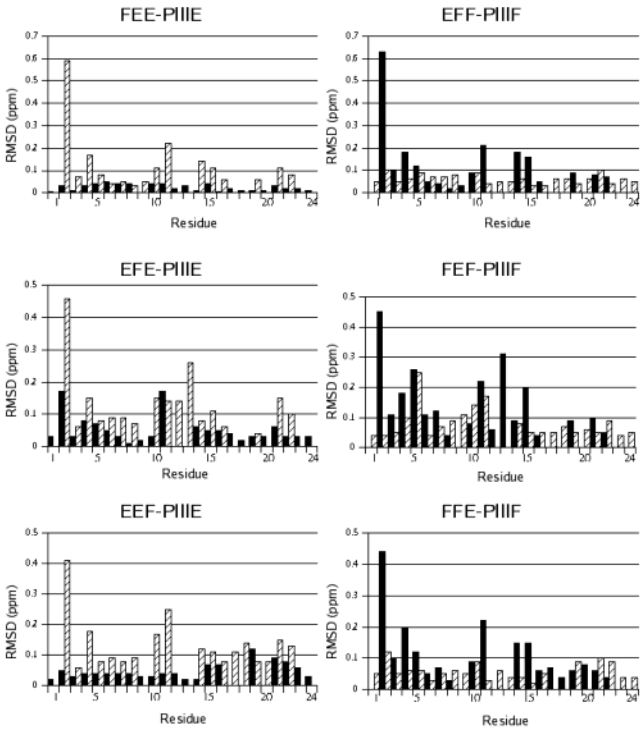

FIGURE 6: Chemical shift RMSD plots for the chimeric ψ-conotoxins. The average RMSD in ppm is shown for all proton signals in each residue as a function of sequence. Black bars indicate comparison with ψ-PIIIE and crosshatched bars indicate comparison with ψ-PIIIF. Data are excluded for cases in which the amino acids being compared are nonidentical.

Figure 6. These data indicate that FEE-PIIIE is in essence identical to ψ-PIIIE in structure aside from the presence of Ser at residue 9 instead of Lys. The chemical shifts of EFE-PIIIE also match up better with ψ-PIIIE than with ψ-PIIIF. There are two main regions of difference between EFE-PIIIE and ψ-PIIIE at residues 2 and 11. Overall, EEF−PIIIE resembles ψ-PIIIE in chemical shift values more than it does ψ-PIIIF; the only differences occur in the regions immediately adjacent to the third loop, and these differences are not large. The chemical shift data for EFF−PIIIF reveal that this peptide most likely has the same conformation in solution as ψ-PIIIF. The chemical shifts of FEF−PIIIF more closely resemble ψ-PIIIF in general than they do ψ-PIIIE. There are some differences, however, near the second loop as well as at C5. The chemical shifts of FFE-PIIIF are essentially identical to those of ψ-PIIIF in the relevant regions. The chemical shifts of the third loop are very similar to ψ-PIIIE.

One interesting difference in structure between ψ-PIIIE and ψ-PIIIF is the occurrence of multiple conformations for the disulfide bridge Cys10−22. The NMR data for ψ-PIIIF are consistent with possible dynamic motion of the side chains of residues C10 and C22 as the β protons of C22 were degenerate in chemical shift and the intraresidue nOe and scalar coupling interactions of C10 are not consistent with a static and staggered conformation for χ^1 for this residue. The chemical shift values of the chimeric peptides were analyzed for the presence of chemical shift degeneracy among the β protons of cysteine residues. The results of this analysis are presented in Table 5. One of the two most interesting aspects of these results is that chemical shift degeneracy occurs only for peptides containing the second loop region derived from ψ-PIIIF (ROFOG). All peptides containing this sequence

Table 5: Occurrence of Chemical Shift Degeneracy in Cysteine Residues among the ψ-PIIIE/ψ-PIIIF Chimeras

	residues
ψ-PIIIE	none
FEE−PIIIE	none
EFE−PIIIE	C10
EEF−PIIIE	none
ψ-PIIIF	C22
EFF−PIIIF	C10, C22
FEF−PIIIF	none
FFE−PIIIF	C10

exhibited chemical shift degeneracy for C10 and/or C22 while none of the peptides containing the analogous region from ψ-PIIIE (RRYOG) exhibited chemical shift degeneracy for cysteine β protons. The other notable aspect is that degeneracy of cysteine β protons is limited to either or both of the residues C10 and C22, both of which are involved in a mutual disulfide bridge.

While the ψ-PIIIF-based mutant FEF−PIIIF did not exhibit chemical shift degeneracy for either C10 or C22, there are indicators of backbone chain dynamics not present in ψ-PIIIF. One such indicator is in the apparent line widths for certain resonances. The protons L6H^N, R11H^N, and C21H^N are all too broad to be observed in two-dimensional NMR spectra collected at 4 °C. Subsequent data collection at 22 °C did allow confirmation of the correct sequence of the peptide, although those signals are still very broad, even at the higher temperature. C21H^N is also broad in ψ-PIIIF, but not to the same degree as was observed in FEF−PIIIF. Another interesting observation derived from the higher temperature study is that the chemical shift of C5H$^\alpha$ is shifted significantly downfield compared to the value observed at the lower temperature. The shift amounts to a $\Delta\delta/\Delta T$ of ~16 ppb/K. Also the $\Delta\delta/\Delta T$ for C5H$^{\beta 2}$ is ~6 ppb/K. The average $\Delta\delta/\Delta T$ for other carbon-bound protons in FEF−PIIIF is a more reasonable value at around 1 ppb/K. These data indicate that the second loop region affects the dynamic mobility of other regions of the peptide.

Chimeras of ψ-PIIIE and ψ-PIIIF: Electrophysiology. The six chimeras were also tested for potency on oocyte-expressed *Torpedo* nAChRs, as the affinity of ψ-conotoxins for the mouse muscle nAChR is too low for a similar study to be carried out on this receptor. The ability of each chimeric peptide to block ACh-gated currents in oocytes expressing *Torpedo* nAChRs is summarized in Figure 7. The apparent IC_{50} values based on these measurements are presented in Table 4.

The results indicate that the third loop region of these ψ-conotoxins appears to be the most important one in determining the difference in inhibitory potency between the peptides. The chimera EEF−PIIIE is significantly less potent than ψ-PIIIE, while the reciprocal chimera, FFE-PIIIF, is significantly more potent than ψ-PIIIF and slightly more potent than ψ-PIIIE as well. In fact, all chimeras in which the third loop is derived from ψ-PIIIE (FFE-PIIIF, FEE-PIIIE, EFE-PIIIE) are similarly potent to ψ-PIIIE.

The first and second loop regions have much less dramatic effects on binding potency. The chimera EFE-PIIIE is only slightly less potent than ψ-PIIIE. The chimera FEE-PIIIE has a slightly greater potency than ψ-PIIIE, suggesting that the positive charge in this loop of ψ-PIIIE (on K9) does not play

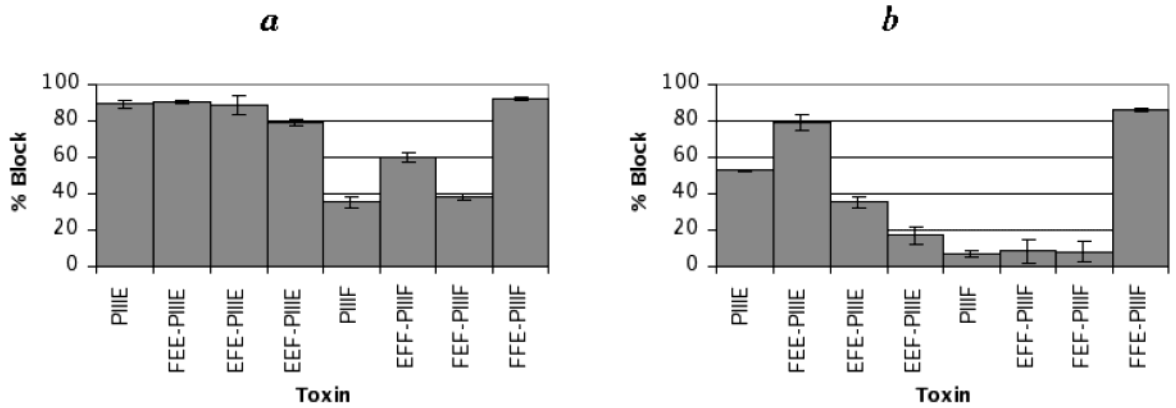

FIGURE 7: Summary of the inhibitory effects of ψ-PIIIE, ψ-PIIIF, and chimeras on ACh-gated currents in oocytes expressing *Torpedo* nAChRs. Results are shown for (a) 10 μM, and (b) 200 nM toxin in the oocyte bath. Each graph is the average of three experiments. The error bars are the standard deviation in the measured data.

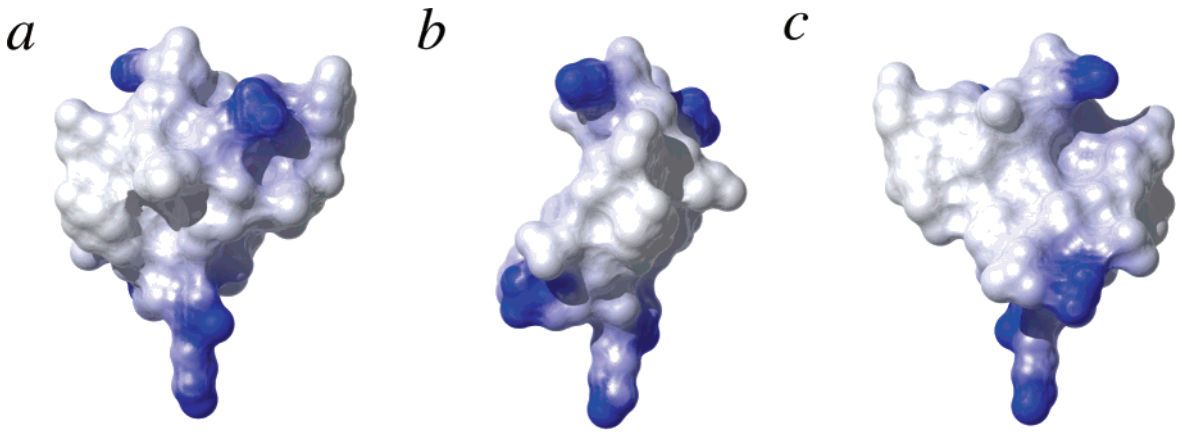

FIGURE 8: Electrostatic surface potential for ψ-conotoxin PIIIF. Blue regions indicate a positive electric potential. The regions of most intense color correspond to a charge of +1 or greater. (a) A view of ψ-PIIIF from the front of the molecule as defined for ψ-PIIIE. (b) Side view of ψ-PIIIF. The front of the molecule is to the right while the back is to the left. (c) The backside of ψ-PIIIF. Note the nonpolar, bulky side chain of L20 on the lower left-hand side. Potential calculations were performed using the SimpleCharge algorithm of MOLMOL 2k.2.

a major role in binding affinity. In addition, the substitutions in loop 2 (which also change the net charge) do not appear to greatly affect the binding of the ψ-conotoxins to the nAChR.

DISCUSSION

The experiments described in this report involved the purification, characterization, and three-dimensional structure determination of ψ-PIIIF, a novel ψ-conotoxin from the venom of *C. purpurascens* specimens collected from the Clipperton Islands. This peptide is homologous to ψ-PIIIE, which was isolated from *C. purpurascens* specimens collected in the Gulf of California and shown in competition binding studies with α-bungarotoxin to noncompetitively bind to nAChRs from *Torpedo* electric organ (*3*). It is therefore assumed that ψ-PIIIF, which inhibits oocyte-expressed *Torpedo* receptors, also does so in a noncompetitive fashion.

Although we cannot eliminate the possibility that other ψ-conotoxins more closely related to ψ-PIIIE are encoded in the genome in the Clipperton Island variant of *C. purpurascens*, ψ-PIIIE and ψ-PIIIF are major components of venom milked from specimens collected at the two localities maintained in identical or, in many cases, the same aquaria. This makes it likely that ψ-PIIIF represents the major form of ψ-conotoxin expressed in the *C. purpurascens* specimens analyzed.

Structure of ψ-PIIIF. Overall ψ-PIIIF has the shape of a lens (see Figure 8). Using the terminology applied to ψ-PIIIE, the front of the molecule is slightly convex while the back of the molecule is slightly concave when viewed from either side. When viewed from the front or back, the molecule has an overall triangular shape. The main body of the peptide is in general well-converged across the ensemble (see Figure 5). The residues showing the most disorder occur at the termini or near the disulfide bridge Cys10−22. Although various measures of the stereochemical quality of the models (Table 2) indicate good stereochemistry, the energy values calculated for ψ-PIIIF are relatively high. Additionally, a fairly high RMSD from distance restraints is observed in the structures and is probably a consequence of the use of the IRMA approach which provides more precise distance restraints with a narrower range of allowed distances than other methodologies. The high energies may result in part from strain inherent to the tightly cross-linked structure of the peptide, however, as unrestrained energy minimization of structures resulting from earlier calculations produced peptides with high energies, albeit significantly lower energies than were observed in the nOe restraint-derived structures.

Two of the three disulfide bridges (Cys4−16 and Cys5−21) exhibit high structural convergence in ψ-PIIIF while the third (Cys10−22) shows a high degree of structural heterogeneity (see Figure 9). Moreover, the NMR data indicate

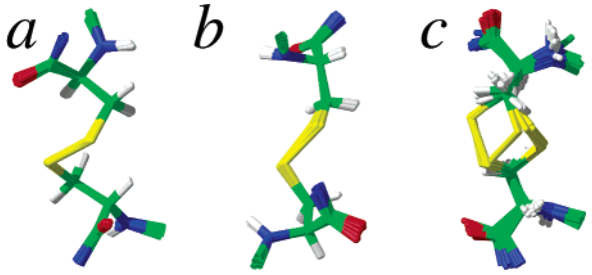

FIGURE 9: Disulfide bridges of ψ-PIIIF. All 17 structures are overlapped for minimal RMSD in atom position for each disulfide bridge. (a) Cys4−16. (b) Cys5−21. (c) Cys10−22.

that this rotational mobility may actually occur in solution for ψ-PIIIF. As was mentioned earlier, the intraresidue nOe data and $^3J_{H\alpha H\beta}$ data for C10 indicate rotational dynamics for the side chain. Also, the β protons of C22 are degenerate in chemical shift; this effect can result from rotational averaging of the chemical shifts for the two protons.

There are three main regions of positive charge density in ψ-PIIIF (see Figures 5 and 8). The first occurs at the N-terminus and may be somewhat disordered. The second occurs on the front face of the peptide near the top at residue R11. The side chain of R11 is well-ordered and aligns along the front face of the peptide, thus stably presenting the positive charge in the context of the surface of the peptide. The final region of positive charge density is near the C-terminus, which appears to be disordered.

Comparison with ψ-PIIIE. Comparison of the structural statistics for ψ-PIIIE (*4*) and ψ-PIIIF indicate that the two ensembles are of similar quality. On the basis of a comparison of sequence and disulfide connectivity (see Figure 1), ψ-PIIIE and ψ-PIIIF are predicted to have very similar backbone conformations in solution. This is confirmed by comparison of the two peptides. Although the general shape of the peptide backbones is similar between ψ-PIIIE and ψ-PIIIF, there are some differences in backbone conformation. Three major regions of divergence in backbone conformation are highlighted by analysis of the backbone atom RMSD of tripeptide fragments between ψ-PIIIE and ψ-PIIIF (data not shown). The first occurs at the N-terminus with the region near the peptide bond between O2 and O3 being the major source of deviation. As residues 2−8 are identical between the two peptides, the most likely cause of the difference between ψ-PIIIE and ψ-PIIIF appears to be the presence in ψ-PIIIE of an imidazolylmethyl side chain for the residue H1. Another region of difference in backbone conformation occurs for residues 9−13, particularly near residues 12 and 13. In ψ-PIIIF, which contains O12, the backbone conformation is consistent within the limitations typically found for proline residues (an observed ϕ value of −76°, close to the ϕ of −65° typical of proline). The analogous residue in ψ-PIIIE (R12) exhibits a ϕ value of −93°. The third major region of difference in peptide backbone structure between ψ-PIIIE and ψ-PIIIF occurs at the C-terminus. Aside from the disposition of the side chain of R24, the C-terminus of ψ-PIIIE is fairly well defined. By contrast, the C-terminus of ψ-PIIIF is less defined. The high degree of divergence seen for the C-terminus of ψ-PIIIF probably does reflect high conformational flexibility as the chemical shifts for the carbon-bound protons of these residues are close to the random coil values (*32*).

The disulfide cores of ψ-PIIIE and ψ-PIIIF show some interesting differences from each other. Examination of the nOe and $^3J_{H\alpha H\beta}$ coupling information indicated similar χ^1 values for C4, C5, C16, and C21 between ψ-PIIIE and ψ-PIIIF. Both the NMR data and the molecular models indicate that the disulfide bridges Cys4−16 and Cys5−21 are structurally static in ψ-PIIIE and in ψ-PIIIF. Yet, despite these four cysteine residues having identical χ^1 conformers, there are large differences in the disulfide bridge conformations for Cys4−16 and Cys5−21. In ψ-PIIIF, Cys4−16 has a disulfide dihedral angle (χ^3) of roughly −65°, while ψ-PIIIE adopts a χ^3 of opposite polarity at +90°. Similarly, Cys5−21 has a χ^3 of +90° in ψ-PIIIE and a χ^3 of −90° in ψ-PIIIF. It is not clear from the models whether the differences in disulfide bridge conformation noted are in any way related to the apparent conformational mobility of the third disulfide bridge.

In addition to effects on backbone conformation, the residue differences between ψ-PIIIE and ψ-PIIIF are expected to affect the polar properties of the surface of the peptide in solution. One difference is in the pattern of basic moiety presentation. ψ-PIIIE is significantly more basic than ψ-PIIIF (six ionizable groups vs four). In Figure 8 are shown surface representations of ψ-PIIIF colored according to electrostatic potential. The "rear" surface of ψ-PIIIF is considerably less polar than the corresponding face of ψ-PIIIE near residue 20. The presence of the alkyl side chain of L20 in ψ-PIIIF has a large effect on both the shape and polar character of that region of the molecule. When viewed from the rear of the molecule a bulge on the surface caused by the aliphatic side chain of L20 is quite apparent when compared to ψ-PIIIE (see Figure 8c). The absence in ψ-PIIIF of the side chain associated with H1 in ψ-PIIIE also has a notable impact on polarity and surface shape near residue 1. In ψ-PIIIF, which contains G1, a small groove between the residues 1−3 and the major body of the peptide is present. In ψ-PIIIE, the side chain of H1 packs close to the body of the peptide rendering this area of the molecule more flat.

Inhibitory Activity of the ψ-Conotoxins. These studies reveal that despite similar toxicity profiles in teleosts (i.e., goldfish), ψ-PIIIE and ψ-PIIIF exhibit different potencies against the mouse and elasmobranch (electric ray) variants of nAChR, the former being about 50 times more potent on both types of receptors. The first step in identifying the structural determinants for these differing potencies was accomplished by synthesizing a series of chimeric peptides containing regions from both ψ-conotoxins. Several general conclusions can be made based on the activity of these chimeras on oocyte-expressed *Torpedo* receptors. The prime determinant of inhibitory potency appears to be the third loop region. Toxins containing the third loop from ψ-PIIIE are more potent than those containing the third loop from ψ-PIIIF. The two peptides differ in three of four positions in this loop, where ψ-PIIIE has the polar sequence -SSAS- and ψ-PIIIF has the more hydrophobic sequence -YNAL-. Thus, the presence of polarity or of low steric bulk in this portion of the peptide may be important for optimal binding to the *Torpedo* receptor. The remaining differences in binding potency from the parent toxins observed among the chimeric peptides were more subtle and therefore not readily interpretable given the limitations in precision of the experiments undertaken.

Conclusions. Interesting observations arise in comparing the sequences and structures of ψ-PIIIE and ψ-PIIIF. The degree of sequence divergence between ψ-PIIIE and ψ-PIIIF is atypically high in comparison to what is usually observed among homologous conotoxins isolated from different snails within a species. The backbone conformations of ψ-PIIIE and ψ-PIIIF show a high degree of similarity as is expected given the sequence homology between the two. In contrast to ψ-PIIIE, however, the third disulfide bridge of ψ-PIIIF appears to undergo dynamic structural fluctuation. Increased dynamics of this bridge is indicated by both the NMR data for the residues C10 and C22 and by the molecular models. The two ψ-conotoxins also differ from each other significantly in steric bulk and polarity near the third loop, a region apparently important in determining the inhibitory potency of the toxins.

The presence of multiple disulfide bridges is an important characteristic of conotoxins. The spacing between cysteine residues and pattern of disulfide bonding has been hypothesized to be the primary determinant of conotoxin global conformation. Disulfide bridges are sometimes located in the core of conotoxin structures. The structural and dynamic properties of disulfide bridges are therefore likely to affect global conformation in the conotoxins. The methods used in this study and in a previous study with ψ-PIIIE directly address the issue of disulfide bridge conformation by resolving data ambiguities that otherwise prevent specification of cysteine conformation. Application of these methods to the ψ-conotoxins has produced data indicating differences between ψ-PIIIE and ψ-PIIIF in the apparent conformational mobility of the third disulfide bridge. The high-resolution structures also indicate that the increased dynamic motion of the third disulfide bridge may result from a difference between ψ-PIIIE and ψ-PIIIF in the structures of their disulfide cores. Study with the chimeric ψ-conotoxins indicate that the second loop affects the dynamic properties of the third disulfide bridge. Although the inhibitory potency shows no apparent correlation with disulfide bridge conformation, differences between ψ-PIIIE and ψ-PIIIF in disulfide bridge conformation are interesting given that both peptides have identical patterns of cysteine occurrence and disulfide bonding.

ACKNOWLEDGMENT

We thank Dr. Robert Schackmann for solid phase synthesis of the peptides and Richard Dela Cruz for help folding and purifying some chimeric peptides. Plasmids encoding the *Torpedo* nAChR were provided by Dr. Jonathan B. Cohen and Dr. Deirdre Sullivan of Harvard University. We also thank the University of Utah Department of Medicinal Chemistry mass spectrometry facility for mass spectral analysis. We express gratitude to the NIH Grants GM48677 (B.M.O.), RR13030 and RR06262 (C.M.I.), and NSF Grant DBI-0002806 for funding NMR instrumentation in the University of Utah Health Sciences NMR Facility.

SUPPORTING INFORMATION AVAILABLE

One table showing full chemical shift assignments for ψ-PIIIF, one table showing the full set of restraints used to calculate the structures, one table showing the parameters used for molecular modeling, one table showing various NMR acquisition parameters, six tables showing the chemical shift values of the chimeras, and one table showing the hydrogen bonds present in the ψ-PIIIF models. This material is available free of charge via the Internet at http://pubs.acs.org.

REFERENCES

1. Olivera, B. M. (1997) *Mol. Biol. Cell. 8*, 2101−2109.
2. Olivera, B. M., Walker, C., Cartier, G. E., Hooper, D., Santos, A. D., Schoenfeld, R., Shetty, R., Watkins, M., Bandyopadhyay, P., and Hillyard, D. R. (1999) *Ann. N. Y. Acad. Sci. 870*, 223−237.
3. Shon, K. J., Grilley, M., Jacobsen, R. B., Cartier, G. E., Hopkins, C., Gray, W. R., Watkins, M., Hillyard, D. R., Rivier, J., Torres, J., Yoshikami, D., and Olivera, B. M. (1997) *Biochemistry 36*, 9581−9587.
4. Van Wagoner, R. M., and Ireland, C. M. (2003) *Biochemistry 42*, 6347−6352.
5. Hopkins, C., Grilley, M., Miller, C., Shon, K. J., Cruz, L. J., Gray, W. R., Dykert, J., Rivier, J., Yoshikami, D., and Olivera, B. M. (1995) *J. Biol. Chem. 270*, 22361−22367.
6. Gray, W. R. (1993) *Protein Sci. 2*, 1732−1748.
7. Bodanszky, M., and Bodanszky, A. (1994) in *The Practice of Peptide Synthesis*, pp 68−69, Springer-Verlag, New York.
8. Atherton, E., and Sheppard, R. C. (1989) in *Solid-Phase Peptide Synthesis*, pp 60, IRL Press, New York.
9. Jeener, J., Meier, B. H., Bachmann, P., and Ernst, R. R. (1979) *J. Chem. Phys. 71*, 4546−4553.
10. Braunschweiler, L., and Ernst, R. R. (1983) *J. Magn. Reson. 53*, 521−528.
11. Rance, M., Sørensen, O. W., Bodenhausen, G., Wagner, G., Ernst, R. R., and Wüthrich, K. (1983) *Biochem. Biophys. Res. Commun. 117*, 479−485.
12. Mueller, L. (1987) *J. Magn. Reson. 72*, 191−196.
13. Smallcombe, S. H., Patt, S. L., and Kiefer, P. A. (1995) *J. Magn. Reson. A 117*, 295−303.
14. States, D. J., Haberkorn, R. A., and Ruben, D. J. (1982) *J. Magn. Reson. 48*, 286−292.
15. Folkers, P. J. M., Folmer, R. H. A., Konings, R. N. H., and Hilbers, C. W. (1993) *J. Am. Chem. Soc. 115*, 3798−3799.
16. Palmer, A. G. III, Cavanagh, J., Byrd, R. A., and Rance, M. (1992) *J. Magn. Reson. 96*, 416−424.
17. Piotto, M., Saudek, V., and Sklenar, V. (1992) *J. Biomol. NMR 2*, 661−665.
18. Cavanagh, J., Fairbrother, W. J., Palmer, A. G. III, and Skelton, N. J. (1996) in *Protein NMR Spectroscopy: Principals and Practice*, pp 175−176, Academic Press, Inc., San Diego.
19. Guntert, P., and Wüthrich, K. (1992) *J. Magn. Reson. 96*, 403−407.
20. Boelens, R., Koning, T. M. G., and Kaptein, R. (1988) *J. Mol. Struct. 173*, 299−311.
21. Boelens, R., Koning, T. M. G., van der Marel, G. A., van Boom, J. H., and Kaptein, R. (1989) *J. Magn. Reson. 82*, 290−308.
22. DeMarco, A., Llinás, M., and Wüthrich, K. (1978) *Biopolymers 17*, 617−636.
23. Hyberts, S. G., Marki, W., and Wagner, G. (1987) *Eur. J. Biochem. 164*, 625−635.
24. Mitchell, S. S., Shon, K. J., Foster, M. P., Davis, D. R., Olivera, B. M., and Ireland, C. M. (1998) *Biochemistry 37*, 1215−1220.
25. Nilges, M., Clore, G. M., and Gronenborn, A. M. (1988) *FEBS Lett. 229*, 317−324.
26. Dauber-Osguthorpe, P., Roberts, V. A., Osguthorpe, D. J., Wolff, J., Genest, M., and Hagler, A. T. (1988) *Proteins 4*, 31−47.
27. Koradi, R., Billeter, M., and Wüthrich, K. (1996) *J. Mol. Graphics 14*, 51−55.
28. Wüthrich, K. (1986) *NMR of Proteins and Nucleic Acids*, Wiley-Interscience, New York.
29. Laskowski, R. A., Rullmann, J. A. C., MacArthur, M. W., Kaptein, R., and Thornton, J. M. (1996) *J. Biomol. NMR 8*, 477−486.
30. Nielsen, K. J., Adams, D., Thomas, L., Bond, T., Alewood, P. F., Craik, D. J., and Lewis, R. J. (1999) *J. Mol. Biol. 289*, 1405−1421.
31. Potts, B. C., and Chazin, W. J. (1998) *J. Biomol. NMR 11*, 45−57.
32. Merutka, G., Dyson, H. J., and Wright, P. E. (1995) *J. Biomol. NMR 5*, 14−24.

BI0272757